

# The quantum roll in $d$ -dimensions and the large- $d$ expansion

Bogdan Mihaila\* and John F. Dawson†

*Department of Physics, University of New Hampshire, Durham, NH 03824*

Fred Cooper‡, Mary Brewster§, Salman Habib\*\*

*Theoretical Division, MS B285, Los Alamos National Laboratory, Los Alamos, NM 87545*

(November 2, 2018)

We investigate the quantum roll for a particle in a  $d$ -dimensional “Mexican hat” potential in quantum mechanics, comparing numerical simulations in  $d$ -dimensions with the results of a large- $d$  expansion, up to order  $1/d$ , of the coupled closed time path (CTP) Green’s function equations, as well as to a post-Gaussian variational approximation in  $d$ -dimensions. The quantum roll problem for a set of  $N$  coupled oscillators is equivalent to a  $(d = N)$ -dimensional spherically symmetric quantum mechanics problem. For this problem the large- $N$  expansion is equivalent to an expansion in  $1/d$  where  $d$  is the number of dimensions. We use the Schwinger-Mahanthappa-Keldysh CTP formalism to determine the causal update equations to order  $1/d$ . We also study the quantum fluctuations  $\langle r^2 \rangle$  as a function of time and find that the  $1/d$  corrections improve the agreement with numerical simulations at short times (over one or two oscillations) but beyond two oscillations, the approximation fails to correspond to a positive probability function. Using numerical methods, we also study how the long time behavior of the motion changes from its asymptotic ( $d \rightarrow \infty$ ) harmonic behavior as we reduce  $d$ .

PACS numbers: 11.15.Pg, 11.30.Qc, 3.65.-w; LANL number: LAUR 3 98-3411

## I. INTRODUCTION

The quantum roll problem is the problem of studying the quantum behavior of a particle starting in an unstable equilibrium at the top of a potential hill and “rolling” down with the constraint  $\langle x \rangle = 0$ . The roll problem recently became relevant to cosmology with the advent of the new inflation model [1]. In that model of the early universe one is interested in determining the slow rollover of the scalar inflaton field in a time evolving semiclassical gravitational field. The quantum mechanics of the slow rollover has been previously studied mostly in perturbation theory or in a mean field approximation (see however [2]). For the one dimensional roll problem, it was found that the mean field approximation broke down before the particle reached the bottom of the well. Thus it is important to find approximations which are valid for longer periods of time. One such approximation is to include the  $1/N$  corrections to the mean field result. Our interest in the quantum mechanical model was due to the fact that for this particular problem one is able to perform numerical simulations at arbitrary  $N$ . This is due to the radial symmetry of the roll problem. If we were

interested instead in studying tunnelling numerically in an  $N$  dimensional anharmonic oscillator, one would be restricted to  $N \leq 5$ , using even the most powerful computers available [3].

This paper is constructed as follows: In section II we state the  $d$ -dimensional quantum roll problem and discuss how to choose initial conditions which allow a smooth transition to the  $N \rightarrow \infty$  limit. In section III we derive a Post-Gaussian variational approximation valid at arbitrary  $N$ . In section IV we review the update equations for the Green’s functions valid up to order  $1/N$ . In section V we compare both approximations to exact numerical simulations. In section VI we study the long time behavior of the two-point function as a function of  $N$ . We reserve the appendices for discussing our numerical methods.

## II. QUANTUM ROLL

The quantum roll problem for an upside down Harmonic oscillator with Hamiltonian  $H = (p^2 - x^2)/2$  is the starting point for our discussion. The solution for the spreading of the wave packet with the constraint  $\langle x \rangle = 0$  is exactly known [1]. For example, if at  $t = 0$  the wave function is Gaussian,  $\psi(x) = \exp\{-x^2/2\}$ , then for  $t > 0$ ,

$$\langle x^2(t) \rangle = 1/2 + \sinh^2(t) .$$

This exponential growth of course does not continue in a bounded potential. In this work we will study the quantum roll for a set of  $N$  coupled oscillators in a “Mexican

---

\*electronic mail: bogdan.mihaila@unh.edu

†electronic mail: john.dawson@unh.edu

‡electronic mail: fcooper@lanl.gov

§electronic mail: me.brew@c3serve.c3.lanl.gov

\*\*electronic mail: habib@lanl.gov

hat" potential where the motion is bounded, as a function of the number of oscillators. We take the Hamiltonian to be of the form,

$$H = -\frac{1}{2}\nabla^2 + V(r), \quad (2.1)$$

where

$$\begin{aligned} \nabla^2 &= \sum_{i=1}^N \frac{\partial^2}{\partial x_i^2}, \quad r^2 = \sum_{i=1}^N x_i^2, \\ V(r) &= \frac{g}{8d} (r^2 - r_0^2)^2. \end{aligned} \quad (2.2)$$

with the Schrödinger equation given by:

$$H \Psi(x_i, t) = i \frac{\partial \Psi(x_i, t)}{\partial t}. \quad (2.3)$$

It is convenient to study this problem in a multidimensional coordinate system with  $d \equiv N$ , using the radial coordinate  $r$  and a set of  $d-1$  angular coordinates. We write the Laplacian as [4,5]:

$$\nabla^2 = \frac{\partial^2}{\partial r^2} + \frac{(d-1)}{r} \frac{\partial}{\partial r} - \frac{L_{d-1}^2}{r^2}, \quad (2.4)$$

where  $L_{d-1}^2$  is the generalized orbital angular momentum operator defined by Louck [4]. We separate the wave function as as radial function times a hyperspherical harmonic:

$$\Psi(x_i, t) = \Psi_{d, [\lambda]}(r, t) Y_{d, [\lambda]}(\Omega), \quad (2.5)$$

then the equation for  $\Psi_{d, [\lambda]}(r, t)$  becomes:

$$H(r, l) \Psi_{d, [\lambda]}(r, t) = i \frac{\partial \Psi_{d, [\lambda]}(r, t)}{\partial t}, \quad (2.6)$$

where

$$H(r, l) = -\frac{1}{2} \left( \frac{\partial^2}{\partial r^2} + \frac{d-1}{r} \frac{\partial}{\partial r} \right) + \frac{l(l+d-2)}{r^2} + V(r).$$

Here  $\lambda$  denotes the set of  $(d-1)$  quantum numbers, including the orbital quantum number  $l$  needed to specify completely the hyperspherical harmonic (see for example [5]).

For the quantum roll problem the potential is given by (2.2). If we start at the top of the hill at  $r = 0$  with a radially symmetric initial state centered at  $r = 0$  then there is no angular momentum and we only have to consider the case  $l = 0$ . The first order derivative term in the Hamiltonian can be eliminated by the substitution,

$$\Phi(r, t) = r^{(d-1)/2} \Psi(r, t), \quad (2.7)$$

in which case, the time dependent Schrödinger equation for  $\Phi$  becomes:

$$H'(r, l) \Phi(r, t) = i \frac{\partial \Phi(r, t)}{\partial t}, \quad (2.8)$$

where

$$H' = -\frac{1}{2} \frac{\partial^2}{\partial r^2} + U(r), \quad (2.9)$$

with an effective one dimensional potential  $U(r)$  given by

$$U(r) = \frac{(d-1)(d-3)}{8r^2} + \frac{g}{8d} (r^2 - r_0^2)^2. \quad (2.10)$$

Using this Hamiltonian we can update  $\Phi$  using symplectic methods, or by solving numerically for the eigenfunctions and eigenvalues and using the expansion:

$$\Psi(r, t) = r^{-(d-1)/2} \sum_n C_n e^{-iE_n t} \Phi_n(r), \quad (2.11)$$

with  $C_n$  being determined from the initial conditions on  $\Psi$  using the orthonormality of the  $\Phi_n(r)$ .

### A. Initial conditions

For most of this paper, we will use for simplicity, Gaussian initial conditions, since they allow for a simple determination of the  $C_n$ . However, in this paper we also want to consider a generalization of the Gaussian variational method discussed in [6], which was found quite robust in describing the time evolution of pulses in classical dynamical systems. This generalized wave function has the ability to approximate in shape an arbitrary spherically symmetric pulse that is monotonically decreasing around  $r = 0$ . This is accomplished by adding one more variational parameter  $\alpha$  which changes the shape of the pulse from flat to peaked, including the Gaussian as the special case  $\alpha = 1$ . Pulses of this form stay coherent for a long time in many nonlinear equations and have been used previously in variational calculations of soliton motion to study soliton blowup. They have the advantage of allowing analytical expressions for the expectation values and thus are ideal for the variational calculation we will consider below.

Thus we will consider at  $t = 0$ , normalized wave functions of the form

$$\begin{aligned} \Psi_{[\alpha]}(r, 0) &= \left[ \frac{2\alpha}{\Omega_d \Gamma[d/(2\alpha)]} \right]^{1/2} \left( \frac{2\alpha G_{[2\alpha]}}{d} \right)^{-d/(4\alpha)} \\ &\times \exp \left( -\frac{d}{4\alpha G_{[2\alpha]}} r^{2\alpha} \right), \end{aligned} \quad (2.12)$$

where  $\Omega_d$  is the angular volume,  $\Omega_d = 2 \pi^{d/2} / \Gamma(d/2)$ , such that we satisfy the normalization condition

$$1 = \Omega_d \int_0^\infty |\Psi_{[\alpha]}(r, 0)|^2 r^{d-1} dr. \quad (2.13)$$

The energy of this state has the form:

$$E(\alpha) = a(\alpha) G_{[2\alpha]}^{-1/\alpha} + e(\alpha) G_{[2\alpha]}^{2/\alpha} + f(\alpha) G_{[2\alpha]}^{1/\alpha}. \quad (2.14)$$

where

$$a(\alpha) = \frac{\alpha}{4} (d + 2\alpha - 2) \left( \frac{2\alpha}{d} \right)^{-1/\alpha} R(2\alpha - 2, \alpha), \quad (2.15)$$

$$e(\alpha) = \frac{g}{8d} \left( \frac{2\alpha}{d} \right)^{2/\alpha} R(4, \alpha), \quad (2.16)$$

$$f(\alpha) = -\frac{g}{4d} r_0^2 \left( \frac{2\alpha}{d} \right)^{1/\alpha} R(2, \alpha), \quad (2.17)$$

and we have defined  $R(\beta, \alpha)$  by:

$$R(\beta, \alpha) = \Gamma\left(\frac{\beta + d}{2\alpha}\right) / \Gamma\left(\frac{d}{2\alpha}\right). \quad (2.18)$$

In particular, for  $\alpha = 1$ , the above initial conditions become

$$\Psi_{[1]}(r, 0) = \left[ \frac{2}{\Omega_d \Gamma(d/2)} \right]^{1/2} \left( \frac{2G_{[2]}}{d} \right)^{-d/4} e^{-\frac{d}{4G_{[2]}} r^2}.$$

We notice that  $G_2/d \equiv G$  where

$$G = \langle x_i^2 \rangle$$

for each  $i$ . Evaluating the energy (2.14) for the Gaussian initial state ( $\alpha = 1$ ), we obtain:

$$E = \frac{g}{8d} [d(d+2)G^2 - 2r_0^2 dG + r_0^4] + \frac{d}{8G}. \quad (2.19)$$

## B. Asymptotic form of the wavefunction for large $d$

The eigenfunctions in the large- $d$  limit are Gaussians times polynomials, where the Gaussians are centered about the minimum of the effective potential of the one-dimensional radial problem. In order to get a uniform overlap at arbitrary  $d$  it is important to choose initial conditions so that the expansion in terms of eigenfunctions is similar at all  $d$ . This requires us to run the couplings as a function of  $d$  so that the overlap is constant up to terms of order  $1/d^2$ . This can be done in several ways that differ by terms of order  $1/d^2$ . The method presented below leads to uniform results even at  $d = 1$  as we change the parameters with  $d$ .

In order to do this we need to examine the asymptotic form of the wave function in the large  $d$  limit, and choose parameters so that in this limit, we do not introduce undesirable numerical errors in the initial decomposition of the wavefunction into eigenmodes. At  $t = 0$ , the initial wave function  $\Psi_0(r)$  is a normalized gaussian centered about the origin:

$$\Psi_0(r) = \mathcal{N} \exp\left\{-\frac{r^2}{4G}\right\},$$

with normalization  $\mathcal{N}$ , such that Eq. (2.13) is satisfied. However the *rescaled* wave function  $\Phi_0(r)$  at  $t = 0$  is given by:

$$\begin{aligned} \Phi_0(r) &= \mathcal{N} r^{(d-1)/2} \exp\left\{-\frac{r^2}{4G}\right\}, \\ &= \mathcal{N} \exp\left\{-\frac{r^2}{4G} + \frac{d-1}{2} \ln r\right\}. \end{aligned}$$

Thus the rescaled wave function, for large  $d$ , can be approximated by a gaussian centered about  $r = \tilde{r}_\infty$ . That is, for large  $d$ ,

$$\Phi_0(r) \approx \mathcal{N} \exp\left\{-\frac{(r - \tilde{r}_\infty)^2}{2G_\infty} + O(1/d)\right\}, \quad (2.20)$$

which defines  $\tilde{r}_\infty$  and  $G_\infty$ . For *all*  $d$ , however, we have:

$$\begin{aligned} \tilde{r} = \langle r \rangle_0 &= \mathcal{N}^2 \Omega_d \int_0^\infty r^d e^{-r^2/2G} dr, \\ &= \sqrt{2G} \left[ \frac{\Gamma((d+1)/2)}{\Gamma(d/2)} \right]. \end{aligned} \quad (2.21)$$

$$\begin{aligned} \langle r^2 \rangle_0 &= \mathcal{N}^2 \Omega_d \int_0^\infty r^{d+1} e^{-r^2/2G} dr, \\ &= \sqrt{dG}. \end{aligned} \quad (2.22)$$

Thus, we define:

$$\frac{G_\infty}{2} = \langle r^2 \rangle - \langle r \rangle^2 = G \left\{ d - 2 \left[ \frac{\Gamma((d+1)/2)}{\Gamma(d/2)} \right]^2 \right\},$$

or

$$G = \frac{G_\infty}{2d - 4 \left[ \frac{\Gamma((d+1)/2)}{\Gamma(d/2)} \right]^2}. \quad (2.23)$$

In the limit when  $d$  goes to infinity, we have

$$G(d) \rightarrow G_\infty, \quad \tilde{r}(d) \rightarrow \tilde{r}_\infty = \sqrt{(d-1)G_\infty}.$$

Now the solution  $\Phi(r, t)$  satisfies Eq. (2.8) with the potential function  $U(r)$  given by Eq. (2.10). In the spectral method, we expand solutions of Schrödinger's equation in eigenvectors of this equation. For large  $d$ , these eigenvectors are centered about the minimum of the potential  $U(r)$ .  $U(r)$  has the expansion,

$$U(r) = U(\bar{r}) + \frac{1}{2} \bar{m}^2 (r - \bar{r})^2 + \dots, \quad (2.24)$$

where  $\bar{r}$  is given by the solution of the equation,

$$\frac{(d-1)(d-3)}{4\bar{r}^4} = \frac{g}{2d} (\bar{r}^2 - r_0^2), \quad (2.25)$$

and  $\bar{m}^2$  by:

$$\begin{aligned}\bar{m}^2 &= \frac{3(d-1)(d-3)}{4\bar{r}^4} + \frac{g}{2d}(3\bar{r}^2 - r_0^2), \\ &= \frac{g}{d}(3\bar{r}^2 - 2r_0^2).\end{aligned}\quad (2.26)$$

We want to make sure that the difference  $\delta r$  between  $\bar{r}$  and  $\tilde{r}$ ,

$$\delta r = \bar{r} - \tilde{r},$$

remain a constant for all  $d$ . This will insure that the overlap integrals for initial values of the coefficients in a secular expansion will remain approximately the same for all values of  $d$ , and thus numerical errors associated with the initial conditions will not effect our results.

We also define  $m^2$  to be the second derivative of  $V(r)$  evaluated at  $r = \bar{r}$ ,

$$m^2 = \left. \frac{d^2 V(r)}{dr^2} \right|_{r=\bar{r}} = \frac{g}{2d}(3\bar{r}^2 - r_0^2), \quad (2.27)$$

then, (2.26) becomes:

$$m^2(d) = \bar{m}^2 - \frac{3(d-1)(d-3)}{4\bar{r}^4}. \quad (2.28)$$

Solving (2.27) for  $r_0$ , substituting into (2.25) and solving for  $g$  gives:

$$g(d) = \frac{d}{\bar{r}^2} \left\{ \bar{m}^2 - \frac{(d-1)(d-3)}{\bar{r}^4} \right\}. \quad (2.29)$$

Holding  $\bar{m}$  fixed means that the frequency of the oscillation remains the same for all  $d$ . Holding  $\delta r$  fixed, means that the overlap between the initial wave function and initial starting values for the solution remains constant for all  $d$ . Thus for *fixed* values of  $\delta r$ ,  $G_\infty$  and  $\bar{m}^2$ , Eqs. (2.21), (2.23), (2.28), and (2.29), determine values for  $G$ ,  $\tilde{r}$ ,  $\bar{r}$ , and  $g$  for all values of  $d$ . Thus in order to keep the same accuracy in our solutions, we need to run the coupling constant  $g(d)$  and the initial width  $G(d)$  as defined above.

We define  $\rho_0(d)$  and  $\tilde{\rho}(d)$  by the ratios,

$$\rho_0(d) = r_0^2/(Gd), \quad \tilde{\rho}(d) = \tilde{r}^2/(Gd),$$

where  $r_0^2$  is calculated from:

$$r_0^2 = \bar{r}^2 \left\{ 1 + \frac{1}{2} \left[ 1 - \frac{\bar{m}^2 \bar{r}^4}{(d-1)(d-3)} \right]^{-1} \right\}. \quad (2.30)$$

Note that in the limit when  $d$  goes to infinity, the various parameters discussed in this section have the limit

$$g(d) \rightarrow g(\infty) = \frac{1}{G_\infty} \left( \bar{m}^2 - \frac{1}{G_\infty^2} \right) \quad (2.31)$$

$$m^2(d) \rightarrow m^2(\infty) = \bar{m}^2 - \frac{3}{4G_\infty^2} \quad (2.32)$$

$$\rho_0(d) \rightarrow \rho_0(\infty) = 1 + \frac{1}{2(1 - \bar{m}^2 G_\infty^2)} \quad (2.33)$$

$$\tilde{\rho}(d) \rightarrow \tilde{\rho}(\infty) = 1 \quad (2.34)$$

We show in Fig. 1 a plot of  $\rho_0(d)$ ,  $\tilde{\rho}(d)$ ,  $m^2(d)$ , and  $g(d)$  for the cases  $G_\infty = 1$ ,  $\delta r = 2$ , and  $m^2 = 2$  and  $m^2 = 21$ . The corresponding initial values are given in Table I and II. These plots show how these parameters flow as a function of  $d$ . This insures that the initial Gaussian wave function would have finite overlap with the infinite  $d$  eigenfunctions. Other choices which differ by terms of order  $1/d^2$  are also possible.

If we are using the spectral method for solving the Schrodinger equation, we need to make sure that the energy of our initial wave packet is not too large compared with the ground state, so that the solution will be valid for long times. In order to estimate the ground state energy it is sufficient to make a harmonic approximation around the minimum of the effective one dimensional potential  $U(r)$ , given by Eq. (2.24). The ground state wave function is

$$\Phi(r) = N \exp \left[ -\frac{\bar{m}}{2} (r - \bar{r})^2 \right], \quad (2.35)$$

where  $N$  is a normalization constant. Correspondingly, the ground state energy is approximately

$$E_0 = U(\bar{r}) + \bar{m}/2. \quad (2.36)$$

We used this result to get a feeling for how to choose our initial conditions. Afterward we determined our parameters from the asymptotic relations, keeping this result in mind.

### III. TIME-DEPENDENT POST-GAUSSIAN VARIATIONAL METHOD

Because of the radial symmetry of the quantum roll problem, it is possible to make a simple generalization of the Gaussian approximation which allows us to track wave packets which have arbitrarily high correlation functions and thus might be more coherent in their behavior in a non-linear potential. These wave packets were used previously [6] to study soliton behavior and blowup in the classical nonlinear Schrödinger equation in arbitrary  $d$ . These wave functions have the property that at  $d = 1$  they give a much better ground state wave function in that the wave function becomes quite flat and can span both wells. At large  $d$  this wave function goes over to the gaussian limit since that is the correct ground state at large  $d$ . Since the analytic large- $d$  expansion is an expansion about a Gaussian, we expect the post-Gaussian variational wave to be compatible with that expansion only at large  $d$ . At small  $d$ , if we use the parameters obtained from the ground state energy, our initial state will be quite different from a Gaussian and not track an initial Gaussian very well in detail. We can, however start with non-Gaussian initial conditions and make direct comparisons numerically.

The time dependent Schrödinger equation can be obtained by varying the Dirac action

$$\Gamma = \int dt \langle \Psi(t) | i\partial/\partial t - H | \Psi(t) \rangle. \quad (3.1)$$

The Schrödinger equation results by asserting that the action  $\Gamma$  be stationary against arbitrary variations of the wave function  $\Psi(r, t)$ . We approximate the *true* wave function  $\Psi(r, t)$  using a generalized Gaussian trial function of [6]

$$\Psi_v(r, t) = \left[ \frac{2\alpha}{\Omega_d \Gamma[d/(2\alpha)]} \right]^{1/2} \left( \frac{2\alpha G_{[2\alpha]}}{d} \right)^{-d/(4\alpha)} \times \exp \left[ -r^{2\alpha} \left( \frac{d}{4\alpha G_{[2\alpha]}} - i\Lambda \right) \right]. \quad (3.2)$$

Correspondingly, the expectation value of  $r^\beta$  is

$$\langle r^\beta \rangle = \left( \frac{2\alpha G_{[2\alpha]}}{d} \right)^{\beta/(2\alpha)} R(\beta, \alpha), \quad (3.3)$$

where  $R(\beta, \alpha)$  is given by Eq. (2.18). In particular for  $\beta = 2\alpha$ ,

$$G_{[2\alpha]} = \langle r^{2\alpha} \rangle.$$

Note that in ref. [6], we considered only the case when  $\alpha = 1$  where

$$G_{[2]} = \langle r^2 \rangle = dG.$$

Using Eq. (3.3), we can calculate the expectation value of the Hamiltonian,  $\langle H \rangle = \langle H_{\text{free}} \rangle + \langle H_{\text{int}} \rangle$ , with

$$\begin{aligned} \langle H_{\text{free}} \rangle &= -\frac{\Omega_d}{2} \times \\ &\int dr r^{d-1} \Psi_v^*(r, t) \left( \frac{\partial^2}{\partial r^2} + \frac{d-1}{r} \frac{\partial}{\partial r} \right) \Psi_v(r, t) \\ &= \alpha(d+2\alpha-2) \left( \frac{d}{4\alpha G} - i\Lambda \right) \langle r^{2\alpha-2} \rangle \\ &\quad - 2\alpha^2 \left( \frac{d}{4\alpha G} - i\Lambda \right)^2 \langle r^{4\alpha-2} \rangle \\ &= \alpha(d+2\alpha-2) \left[ \left( \frac{d}{4\alpha G} \right)^2 + \Lambda^2 \right] \\ &\quad \left( \frac{2\alpha G}{d} \right)^{2-\frac{1}{\alpha}} \Gamma_{(2\alpha-2, \alpha)} \end{aligned} \quad (3.4)$$

and

$$\begin{aligned} \langle H_{\text{int}} \rangle &= \Omega_d \int \Psi_v^*(r, t) V(r) \Psi_v(r, t) r^{d-1} dr \\ &= \frac{g}{8d} \langle r^4 \rangle - \frac{g}{4d} r_0^2 \langle r^2 \rangle + \frac{g}{8d} r_0^4. \end{aligned} \quad (3.5)$$

We also find the expectation value of  $i\partial/\partial t$  as

$$\begin{aligned} \langle i\partial/\partial t \rangle &= \frac{i}{2} \Omega_d \int \left[ \Psi_v^* \frac{\partial \Psi_v}{\partial t} - \frac{\partial \Psi_v^*}{\partial t} \Psi_v \right] r^{d-1} dr \\ &= -G_{[2\alpha]} \dot{\Lambda}, \end{aligned} \quad (3.6)$$

so the effective action can be written as:

$$\Gamma = \int dt \left\{ -G_{[2\alpha]} \dot{\Lambda} - a(\alpha) G_{[2\alpha]}^{-1/\alpha} - b(\alpha) G_{[2\alpha]}^{2-1/\alpha} \Lambda^2 - e(\alpha) G_{[2\alpha]}^{2/\alpha} - f(\alpha) G_{[2\alpha]}^{1/\alpha} \right\}, \quad (3.7)$$

where the coefficients  $a(\alpha)$ ,  $e(\alpha)$  and  $f(\alpha)$  are given by Eqs. (2.15, 2.16, 2.17). In addition we have introduced

$$b(\alpha) = a(\alpha) \left( \frac{4\alpha}{d} \right)^2. \quad (3.8)$$

The variational equations of motion are obtained from

$$\begin{aligned} \frac{\delta \Gamma}{\delta \Lambda} &= \dot{G}_{[2\alpha]} - 2b(\alpha) G_{[2\alpha]}^{2-1/\alpha} \Lambda = 0, \\ \frac{\delta \Gamma}{\delta G_{[2\alpha]}} &= -\dot{\Lambda} + \frac{a(\alpha)}{\alpha} G_{[2\alpha]}^{-1-1/\alpha} \\ &\quad - b(\alpha) \left( 2 - \frac{1}{\alpha} \right) G_{[2\alpha]}^{1-1/\alpha} \Lambda^2 \\ &\quad - \frac{2e(\alpha)}{\alpha} G_{[2\alpha]}^{-1+2/\alpha} - \frac{f(\alpha)}{\alpha} G_{[2\alpha]}^{-1+1/\alpha} = 0. \end{aligned} \quad (3.9)$$

Note that Eq. (3.9) can be solved for  $\Lambda$ . We get

$$\Lambda = \frac{1}{2b(\alpha)} \dot{G}_{[2\alpha]} G_{[2\alpha]}^{-2+1/\alpha}. \quad (3.11)$$

Since the effective action is stationary against variation of the trial wave function  $\Psi_v(t)$ , the equations of motion (3.9, 3.10) guarantee energy conservation:

$$\begin{aligned} E/d &= a(\alpha) G_{[2\alpha]}^{-1/\alpha} + b(\alpha) G_{[2\alpha]}^{2-1/\alpha} \Lambda^2 \\ &\quad + e(\alpha) G_{[2\alpha]}^{2/\alpha} + f(\alpha) G_{[2\alpha]}^{1/\alpha}. \end{aligned} \quad (3.12)$$

The conservation provides a first integral of the motion and gives us a non-linear differential equation to solve in terms of  $G_{[2\alpha]}$  and the initial energy.

Stationary solutions are obtained by requiring  $\dot{G}_{[2\alpha]} = \dot{\Lambda} = 0$ . Then, from Eqs. (3.9, 3.10) we obtain  $\Lambda = 0$  and an equation for  $G_{[2\alpha]}$

$$2e(\alpha) G_{[2\alpha]}^{3/\alpha} + f(\alpha) G_{[2\alpha]}^{2/\alpha} - a(\alpha) = 0. \quad (3.13)$$

The energy of this stationary solution is:

$$\frac{E(\alpha)}{d} = a(\alpha) G_{[2\alpha]}^{-1/\alpha} + e(\alpha) G_{[2\alpha]}^{2/\alpha} + f(\alpha) G_{[2\alpha]}^{1/\alpha}.$$

By minimizing this energy with respect to  $G_{[2\alpha]}$  and  $\alpha$  we get the best estimate of the ground state wave function for this class of trial wave functions. We must remember that we expect the actual ground state wave function to have its support at  $\bar{r}$  and not around zero. This generalized approximation has the feature that as  $d \rightarrow \infty$ ,  $\alpha_c \rightarrow 1$ .

First let us look at the ground state wave function at  $d = 1$ ,  $g_\infty = 1$ , which, from Table I, corresponds

to  $g = 0.232$  and  $r_0 = 2.9359$ . We compare the variational wave function and ground state energy with the best Gaussian result. Minimizing the energy with respect to the parameters  $G_{[2\alpha]}$  and  $\alpha$ , we find that the optimal parameters are:

$$\alpha_c = 5.25774; \quad G_{[2\alpha_c]} = 152039., \quad (3.14)$$

leading to a normalized wave function given by:

$$\psi(r) = 0.134818 \exp \left\{ -6.25428 \times 10^{-07} r^{10.515483} \right\},$$

corresponding to an energy of  $E(\alpha_c) = -1.05847$ . In comparison, the Gaussian approximation ( $\alpha = 1$ ) leads to the results:

$$\alpha = 1.0; \quad G_{[2]} = 2.95542, \quad (3.15)$$

with a wave function given by:

$$\psi(r) = 0.232058 \exp \left\{ -0.16918 r^2 \right\}$$

corresponding to an energy of  $E(\alpha = 1) = -0.67531$ . A comparison of these two wave functions is found in Fig. 2. Thus the more general wave function has support over both wells and does considerably better for the energy.

Because of this wider support, the post-Gaussian approximation does a better job in reproducing the amplitude of the excursions in the time dependent problem when compared to the Gaussian approximation even though it does not represent the early time evolution. At larger  $d > 10$  when  $\alpha$  becomes closer to unity then the entire evolution is modelled better by this type of trial wave function. This is seen in Fig. 3. We can also compare the generalized Gaussian trial wave function result with a numerical simulation starting from the non-Gaussian initial conditions using the split operator technique described in [7]. The results at two different  $d$ 's are shown in Figs. 4. Again we see that we need  $d \geq 10$  for this approximation to give reasonable results.

#### IV. LARGE- $N$ EXPANSION

The large- $N$  ( $d$ ) expansion for the  $d$ -dimensional anharmonic oscillator is the zero space dimensional limit of the  $\phi^4$  field theory formalism discussed in ref. [8]. The effective action to order  $1/d$  is given by [here we use the field theory notation of ref. [8]:  $d \rightarrow N$ ,  $g \rightarrow \lambda$ , and  $\mu^2 \rightarrow -gr_0^2/(2d)$ ],

$$\begin{aligned} \Gamma[\chi, x_i] = & \int_C dt \left\{ \frac{1}{2} \sum_i \left\{ \dot{x}_i^2(t) - \chi x_i^2(t) \right\} + \frac{iN}{2} \ln[G_0^{-1}(t, t)] \right. \\ & \left. + \frac{N\chi^2(t)}{2\lambda} - \frac{N\mu^2\chi(t)}{\lambda} + \frac{i}{2} \ln[D^{-1}(t, t)] \right\}, \end{aligned} \quad (4.1)$$

where  $G_{ab}^{-1}(t, t')$  and  $D^{-1}(t, t')$  are the inverse propagators for  $x_i$  and  $\chi$ , given (for  $\langle x_i \rangle = 0$ ) by

$$\begin{aligned} G_{ab}^{-1}(t, t') &= \left\{ \frac{d^2}{dt^2} + \chi(t) \right\} \delta_C(t, t') \delta_{ab} \\ &\equiv G_0^{-1}(t, t') \delta_{ab}, \end{aligned} \quad (4.2)$$

$$D^{-1}(t, t') = -\frac{N}{\lambda} \delta_C(t, t') - \Pi(t, t'), \quad (4.3)$$

$$\Pi(t, t') = -\frac{i}{2} \sum_{a,b=1}^N G_{ab}(t, t') G_{ba}(t', t). \quad (4.4)$$

Here  $\delta_C(t, t')$  is the closed time path delta function. The auxiliary variable  $\chi(t)$  obeys the constraint equation given by

$$\chi(t) = \mu^2 + \frac{\lambda}{2N} \sum_{a=1}^N \frac{1}{i} \mathcal{G}_{aa}(t, t), \quad (4.5)$$

and where the full  $x_i$  propagator  $\mathcal{G}(t, t')$  and self energy  $\Sigma(t, t')$  to order  $1/N$  are given by

$$\begin{aligned} \mathcal{G}_{ab}(t, t') &= G_{ab}(t, t') \\ &- \sum_{c,d=1}^N \int_C dt_1 \int_C dt_2 G_{ac}(t, t_1) \Sigma_{cd}(t_1, t_2) G_{db}(t_2, t') \\ \Sigma_{cd}(t, t') &= i G_{cd}(t, t') D(t, t'). \end{aligned} \quad (4.6)$$

These equations are also derived in (2.18–2.22) of ref. [8]. In order to solve for  $D(t, t')$ , we first write

$$\frac{N}{\lambda} D(t, t') = -\delta_C(t, t') + \frac{N}{\lambda} \Delta D(t, t'). \quad (4.7)$$

Then we find that  $\Delta D(t, t')$  satisfies the integral equation,

$$\Delta D(t, t') = \frac{\lambda}{N} \Pi(t, t') - \int_C dt'' \Pi(t, t'') \Delta D(t'', t'), \quad (4.8)$$

in agreement with (2.13–2.16) of Ref. [8]. We are now in a position to solve these coupled equations for the motion of  $\mathcal{G}_{ab}(t, t')$  and  $\chi(t)$  for given initial conditions. We solve Eq. (4.5) simultaneously with (4.6) and (4.8), using the Chebyshev expansion technique of appendices A and B of ref. [9].

#### V. COMPARISON OF APPROXIMATIONS WITH EXACT NUMERICAL SIMULATIONS.

In this section we will compare the exact solution (determined numerically) with both the variational method and the large- $N$  expansion. In order to have a smooth  $d \rightarrow \infty$  transition, we will allow our parameters to run as a function of  $d$  as described above. We use the set of parameters listed in tables I and II, which correspond to the choice of  $G_\infty = 1$ ,  $\delta r = 2$ , and the two cases  $\bar{m}^2 = 2$ ,  $g_\infty = 1$  and  $\bar{m}^2 = 21$ ;  $g_\infty = 20$ , respectively. First let us

discuss Gaussian initial conditions. In Figs. 5 we present the results for  $\langle r^2/d \rangle$  which correspond to  $g_\infty = 1$ . We find that at short times (less than 2 oscillations) the calculation which includes  $1/N$  corrections tracks the exact result the closest, however when it starts deviating from the exact result it can lead to a negative expectation value. This is evidence that the next to leading order large- $N$  approximation does not correspond to a positive definite probability function. At leading order, the large- $N$  approximation is equivalent to a Gaussian wave function (or density matrix) and all the expectation values of even moments of operators are positive. This problem of not having a positive definite probability associated with this type of approximation scheme also arises if we consider approximations which are exact truncations of the Green's function hierarchy [10] at the level of the connected four point function.

The leading order in large- $N$  calculation is closer in amplitude to the exact result than the Hartree variational approximation. These latter two approximations do not suffer from the illness of the next to leading large- $N$  approximation. We see that all the approximations approach the exact one as  $d \rightarrow \infty$  as they must. In Figs. 6 we see the same type of behavior at a larger value of  $g_\infty = 20$ . The main difference here is that the time scale for a single oscillation has been reduced, but the behavior in terms of the oscillation time scale is similar to the previous case.

We have also compared the post-Gaussian variational approximation for Gaussian initial data. This comparison is shown in Figs. 3. Here, the initial states are clearly different so we have normalized the two wave functions so as to have the same value for  $\langle r^2 \rangle$ . What is interesting here is that the post-Gaussian approximation gives a better approximation for the amplitude of the oscillation, which "cures" the previously found failure of the Gaussian approximation to reach the bottom of the Mexican Hat potential in one dimension. To truly test the post-Gaussian approximation we used non-Gaussian initial conditions pertaining to the value of  $\alpha = \alpha_c$  found by minimizing the ground state energy. To obtain our numerical results here, it was not possible to use the eigenfunction method because of the number of eigenfunctions required to approximate this type of wave function. Instead we used the split operator technique of [7]. As shown in Figs. 4 we see that the post-Gaussian approximation does quite well with the amplitude of the oscillation, but only at large  $d \geq 10$  does it start getting the frequency of oscillations correct.

## VI. LONG-TIME BEHAVIOR OF $\langle r^2 \rangle$ AS A FUNCTION OF $d$ .

At large  $d$  the effective one dimensional radial potential is very deep and becomes harmonic for oscillations around the minimum. Thus as  $d \rightarrow \infty$  an initial Gaus-

sian wave packet should stay gaussian, because the gaussians are coherent states of the harmonic oscillator. However, the solutions for finite dimension  $d$  can not be expected to maintain the coherence of the original Gaussian state over long time intervals. It is of interest to observe the actual long-time behavior of the solutions that arise from Gaussian initial conditions when the potential is not purely quadratic.

The method of eigenfunction expansion can be used to calculate the solution over large time intervals. The accuracy of the long-term behavior is limited primarily by the accuracy of the eigenvalues, so the tolerance of the eigenvalue calculation was reduced until numerical convergence of the solution was observed over the time intervals of interest.

The few examples that we consider in this paper show a surprising variety of long-time behaviors. In Figs. 7-8 we show the evolution of  $G_2 = \langle r^2/d \rangle$  over a time interval sufficiently long to capture the characteristic behavior of that particular solution.

In Fig. 7 we notice that as we increase  $d$  we gradually approach the limiting form of oscillation in an harmonic well. In the case  $d = 1$ ,  $\bar{m}^2 = 2$ , (Fig. 7a  $G_2$  is dominated by the contribution of the lowest frequency and so appears as a perturbation of a simple oscillation with frequency equal to the energy difference between the ground and first excited states. The solution itself contains one dominant peak with a few smaller peaks. As we increase  $d$  the potential gets more harmonic and simple harmonic motion of  $G_2$  is observed. At larger  $g_\infty$ , as seen in Fig. 8, more complicated behavior can be seen.

In the case  $d = 1$ ,  $\bar{m}^2 = 21$ , (Fig. 8b) there is a significant modulation of the amplitude, so that at regular intervals there is a much reduced oscillation of  $G_2$ . The solution typically has several (2-3) peaks of similar size.

In the other cases in Fig. 8, there is always significant amplitude modulation so that there may be brief or in some cases ( $d = 10$  and  $20$ ,  $\bar{m}^2 = 21$ ), extended periods when the amplitude of the oscillation is an order of magnitude less than the initial oscillation. The oscillation always returns to a significant fraction (50-90%) of the initial oscillation, even after extended periods of reduced amplitude. The pattern of amplitude modulation can be quite complex. The solutions in general have a number of major peaks, from a minimum of 3 up to 12, indicating the contributions from higher eigenstates. However, in some cases the coherence of the initial Gaussian state may be maintained for a significant length of time. For example, in the case  $d = 20$ ,  $\bar{m}^2 = 2$ , the coherent state is maintained approximately for 10 oscillations at the fundamental frequency. For this large value of  $g$  we expect that one needs to get to very large values of  $d \geq 100$  before the asymptotic behavior seen in Fig. 7d will be reached.

## VII. CONCLUSIONS

In this paper we have studied the behavior of  $G_2 = \langle r^2/d \rangle$  for Gaussian and non-Gaussian initial data for the quantum roll in  $d$  dimensions. We found that as  $d \rightarrow \infty$ ,  $G_2$  became more harmonic in behavior as expected. We compared the exact numerical data with two variational approximations (Gaussian and Post Gaussian) for the wave function as well as the leading and next to leading order approximations in the large  $d$  expansion for the Green's functions. We found that all these approximations converged to the exact result as  $d \rightarrow \infty$ . At short times (less than 2 oscillations) the next to leading order large  $d$  approximation was the most accurate one. However when this approximation started diverging from the exact result, it broke down in a serious fashion in that  $G_2$  became negative. This unexpected result is related to the fact the large  $d$  expansion for the expectation values may not necessarily correspond to a positive definite probability when truncated at any finite order in  $1/d$ . At lowest order, however the approximation is equivalent to a Gaussian density matrix and does not have this defect. Variational approximations to the wave function by their very nature never have this defect. Recently [10] we have seen that in a related approximation, namely truncating the equal times connected Green's function at the four point function level,  $G_2$  is not positive definite. Thus we feel that truncating the hierarchy of Green's functions in various ways might always have this problem, apart from the Gaussian case. This leads us to suspect that a higher order variational approach will be necessary if we want to include scattering corrections to mean field theory and also look at long time behavior. This will be the subject of a future paper. For astrophysical applications of the quantum roll problem, one is only interested in getting the correct result to the bottom of the potential, after which particle production leads to dissipative effects as one oscillates at the correct new minimum. For this purpose, keeping the next to leading order in large  $N$  definitely improves the mean field result.

## VIII. ACKNOWLEDGEMENTS

The work by B.M. and J.F.D. at UNH is supported in part by the U.S. Department of Energy under grant DE-FG02-88ER40410. B.M. and J.F.D. thank the Theory Group (T-8) at LANL for hospitality during the course of this work. J.F.D. would also like to thank the Nuclear Theory Center at Indiana University for hospitality during some of this work.

## APPENDIX A: NUMERICAL APPROACH

### 1. Analytical Preliminaries

The time-dependent Schrödinger equation

$$\left\{ -\frac{1}{2} \frac{\partial^2}{\partial r^2} + U(r) \right\} \phi = i \frac{\partial \phi}{\partial t} \quad (\text{A1})$$

where  $U(r)$  is given by (2.10),

$$U(r) = \frac{(d-1)(d-3)}{8r^2} + \frac{g}{8d}(r^2 - r_0^2)^2, \quad (\text{A2})$$

is solved by the method of eigenfunction expansion. Taking a Fourier transform in time, we have the eigenvalue problem

$$-\frac{1}{2} \Phi'' + U \Phi = E \Phi \quad (\text{A3})$$

on the half-line  $r > 0$ . The boundary conditions are finiteness at the origin and the normalization condition,

$$\int_0^\infty |\Phi(r)|^2 dr = 1. \quad (\text{A4})$$

The numerical solution of this eigenvalue problem is described in the next section. The value of the wave function at  $t = 0$  is given by:

$$\phi(r, 0) = \phi_0(r) = A r^{(d-1)/2} \exp(-r^2/4G), \quad (\text{A5})$$

where  $A$  is a normalization constant depending on  $G$  and  $d$ . So the initial-value problem is solved by the expansion

$$\phi(r, t) = \sum_{j=0}^{\infty} c_j \exp(-iE_j t) \Phi_j(r) \quad (\text{A6})$$

where the coefficients are determined by quadrature

$$c_j = \int_0^\infty \phi_0(r) \Phi_j(r) dr. \quad (\text{A7})$$

To evaluate a particular moment of the solution without determining the full spatial solution, we take the moment of the expansion. Thus we may calculate the second moment as follows

$$\langle r^2 \rangle = \sum_{j,k=0}^{\infty} a_{j,k} c_j c_k \cos(E_j - E_k)t, \quad (\text{A8})$$

where

$$a_{j,k} = \int_0^\infty r^2 \Phi_j(r) \Phi_k(r) dr. \quad (\text{A9})$$



## 2. Numerical Solution of Eigenvalue Problem

### a. Discretization

The ordinary differential equation (2) is discretized using a compact finite difference scheme of second-order accuracy. This scheme allowed the easy use of a nonuniform mesh near the origin, which was needed especially in the lower-dimensional cases ( $d < 10$ ) to achieve the desired accuracy. The nonuniform grid  $\{r_n\}$  was created by transforming the independent variable by the formula

$$r = \frac{s^b}{(1+s)^{(b+1)}} \quad (\text{A10})$$

where  $b = 2/(d-3)$  and then using a uniform grid  $[h, 2h, \dots, L]$  in the variable  $s$ . The discretized equations are then

$$\frac{u_{n+1} - u_n}{r_{n+1} - r_n} = \frac{w_{n+1} + w_n}{2},$$

and

$$-\frac{1}{2} \left( \frac{w_{n+1} - w_n}{r_{n+1} - r_n} \right) + \left( \frac{U(r_{n+1}) + U(r_n)}{2} - E \right) \left( \frac{u(r_{n+1}) + u(r_n)}{2} \right) = 0.$$

The boundary conditions at the singular points 0 and  $\infty$  were imposed by specifying  $w = 0$  at the leftmost grid point and  $u = 0$  at the rightmost grid point. The parameters  $h$  and  $L$  were adjusted until sufficient accuracy was achieved, as described in the next section.

### b. Eigensolver

In matrix notation we have  $Ax = EBx$ , where  $x$  is a vector containing the  $u$  and  $w$  values at the grid points. This is a generalized eigenvalue problem and the matrix  $B$  is singular. We can formally convert this to a regular eigenvalue by inverting  $A$ , (although we will never actually invert  $A$  in practice.) We then have  $A^{-1}Bx = \lambda x$ , where  $\lambda = E^{-1}$ . This eigenvalue problem was solved for a specified number (16 usually) of the largest eigenvalues by the method of Arnoldi factorization [11], which is an iterative method and so is very fast provided matrix vector multiplication can be carried out quickly. MATLAB routines were used for the Arnoldi factorization as well as an incomplete L-U factorization of the matrix  $A$  that was used to quickly evaluate the matrix-vector products  $A^{-1}Bx$ .

Convergence of the solution was confirmed by testing the orthogonality of the eigenvectors and by computing the energy of the eigenfunctions from the formula

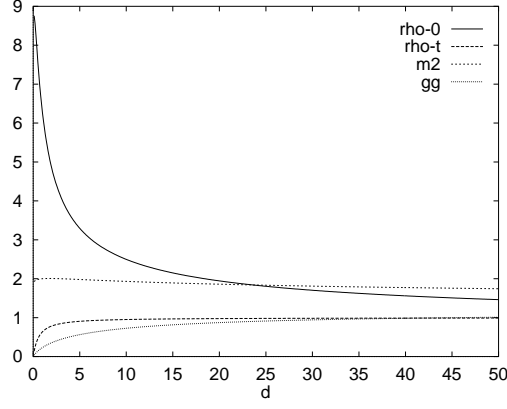
$$E = \int_0^\infty \left\{ \frac{1}{2} \left| \frac{\partial \Phi(r)}{\partial r} \right|^2 + V(r) |\Phi(r)|^2 \right\} dr.$$

The size of the interval, as determined by  $L$ , and the mesh spacing, as determined by  $h$ , that were required to achieve an accuracy of  $10^{-3}$  was highly dependent on the number of eigenvalues being determined and to a lesser extent on the dimension  $d$ . At most 4096 grid points were required in the worst case of 32 eigenfunctions with  $d = 20$  — usually 1024 grid points were sufficient.

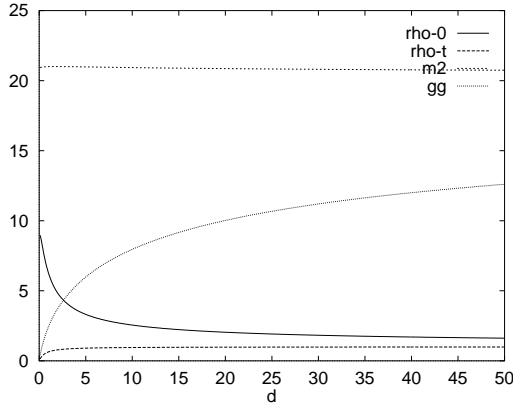
## 3. Solving the Initial-Value Problem

To solve the initial-value problem, the only remaining step is to evaluate the integrals (A7). This is done by using the trapezoidal rule. The accuracy of the quadrature was verified by reconstructing the initial condition and the mesh refined until an accuracy of  $10^{-3}$  was achieved. The integrals (A9) were evaluated similarly.

- 
- [1] A. H. Guth and S.-Y. Pi, Phys. Rev. D **32**, 1899 (1985); F. Cooper, K. Milton, L. M. Simmons, Jr., Phys. Rev. D **32**, 2056 (1985); F. Cooper, S.-Y. Pi and P. Stancioff, Phys. Rev. D **34**, 383 (1986).
  - [2] G. J. Cheetham and E. J. Copeland, Phys. Rev. D **53**, 4125 (1996); gr-qc/9503043.
  - [3] B. Mihaila, J. F. Dawson, F. Cooper, and S. Habib. “Dynamics of the O(N) Model,” (In preparation).
  - [4] J. D. Louck, J. Mol. Spect. **4**, 298 (1960).
  - [5] J. P. Blaizot and G. Ripka, “Quantum Theory of Finite Systems,” (MIT Press, Cambridge, MA, 1986).
  - [6] F. Cooper, H. Shepard, C. Lucheroni and P. Sodano, Physica D **68** 344 (1993).
  - [7] M. R. Hermann and J. A. Fleck, Jr., Phys. Rev. A **38**, 6000 (1988).
  - [8] F. Cooper, S. Habib, Y. Kluger, E. Mottola, J. P. Paz, P. R. Anderson, Phys. Rev. D **50**, 2848 (1994); hep-ph/9405352.
  - [9] B. Mihaila, J. F. Dawson, and F. Cooper, Phys. Rev. D **56**, 5400 (1997); hep-ph/9705354.
  - [10] Luis Bettencourt (private communication) and L. Bettencourt and F. Cooper (In preparation).
  - [11] G. H. Golub and C. F. Van Loan, “Matrix Computations,” (Johns Hopkins University Press, second edition, Baltimore, 1989).



(a)  $G_\infty = 1$ ,  $\delta r = 2$ , and  $\bar{m}^2 = 2$ .



(b)  $G_\infty = 1$ ,  $\delta r = 2$ , and  $\bar{m}^2 = 20$ .

FIG. 1. Plots of  $\rho_0$ ,  $\tilde{\rho}$ ,  $g$ , and  $m^2$  vs  $d$ , for two sets of parameters.

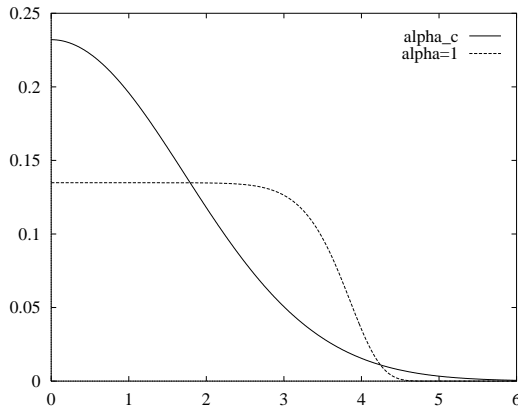
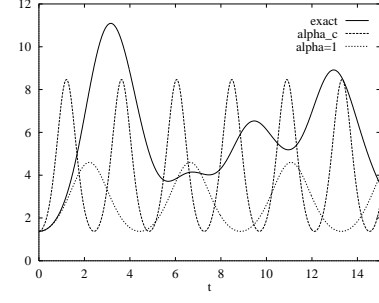
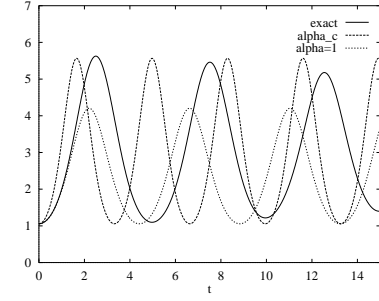


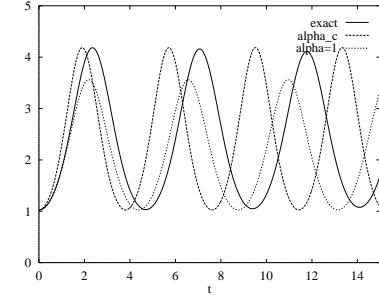
FIG. 2. Gaussian versus generalized Gaussian wave functions, for  $g_\infty = 1$  and  $d = 1$  with  $r_0 = 2.9359$ .



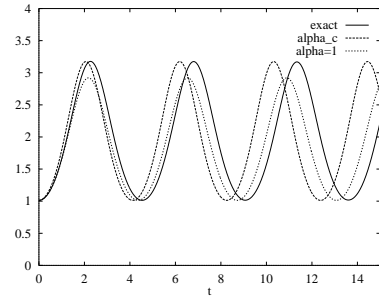
(a)  $d=1$



(b)  $d=5$

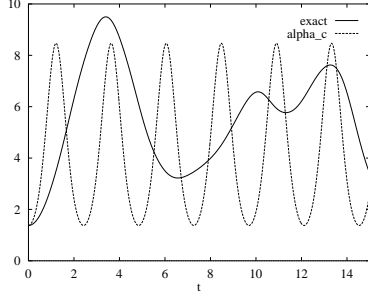


(c)  $d=10$

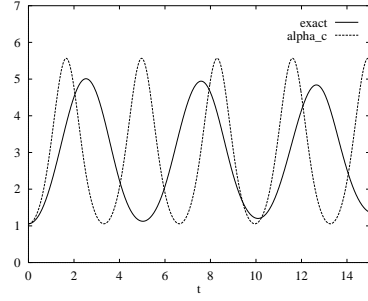


(d)  $d=20$

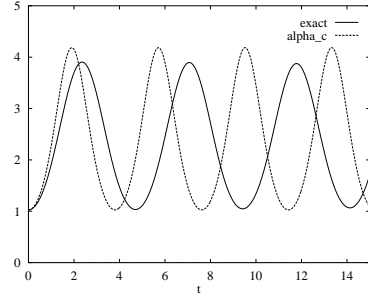
FIG. 3. Gaussian initial conditions with  $g_\infty = 1$ . Here we compare the exact results with both the post-Gaussian approximation normalized to  $\langle r^2 \rangle$  and the Gaussian approximation.



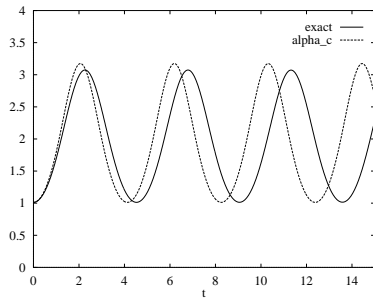
(a)  $d=1$



(b)  $d=5$

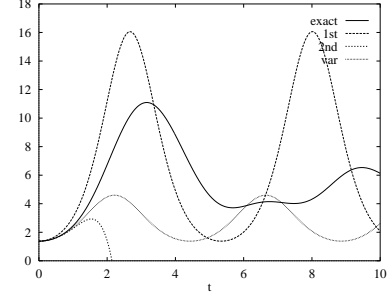


(c)  $d=10$

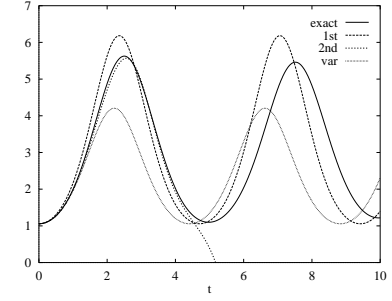


(d)  $d=20$

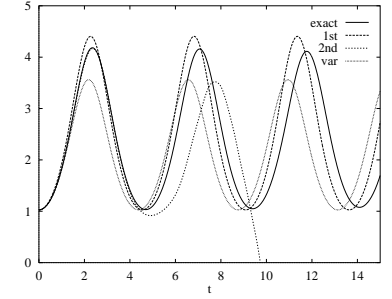
FIG. 4. Post-Gaussian initial conditions with  $g_\infty = 1$ . Here we compare the exact results with the Post Gaussian approximation with  $\alpha_c$  fixed by minimizing the ground state energy.



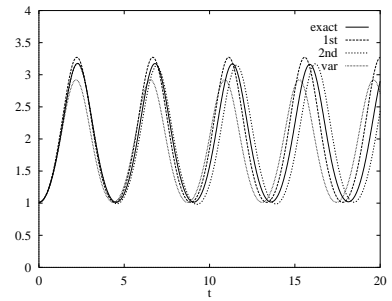
(a)  $d=1$



(b)  $d=5$

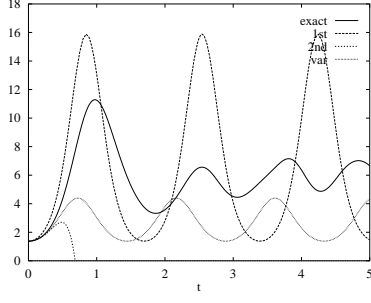


(c)  $d=10$

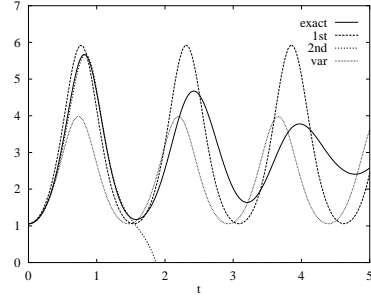


(d)  $d=20$

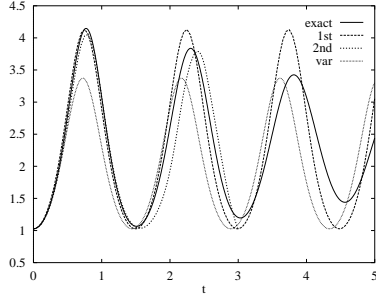
FIG. 5. Gaussian initial conditions with  $g_\infty = 1$ . Here we compare exact result with the leading and next to leading order large- $N$  approximation and to the Gaussian approximation.



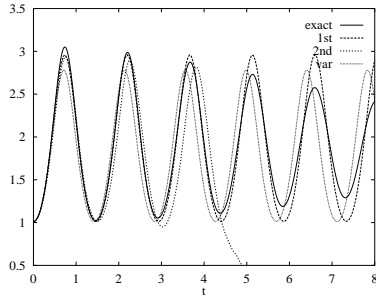
(a)  $d=1$



(b)  $d=5$

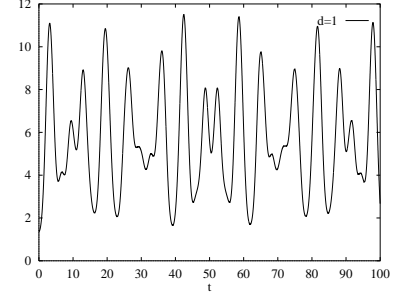


(c)  $d=10$

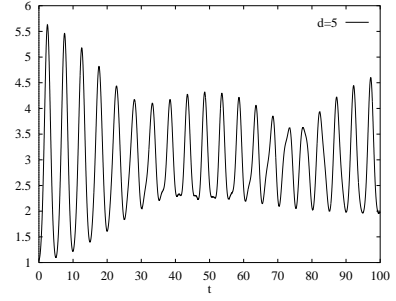


(d)  $d=20$

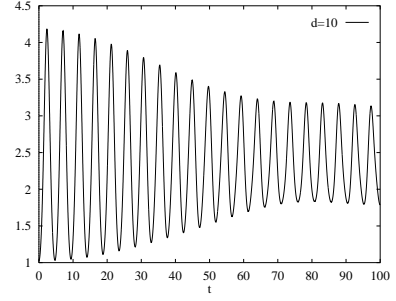
FIG. 6. Gaussian initial conditions with  $g_\infty = 20$ . Similar to Fig. 5 we notice that the next to leading order large- $N$  approximation becomes unstable for small  $d$  at modest time scales.



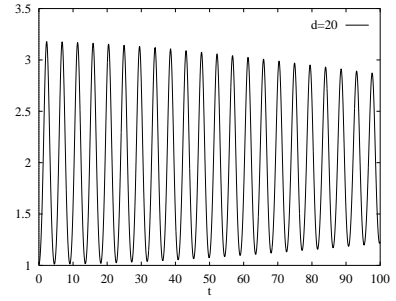
(a)  $d=1$



(b)  $d=5$

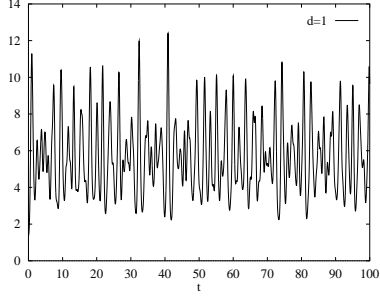


(c)  $d=10$

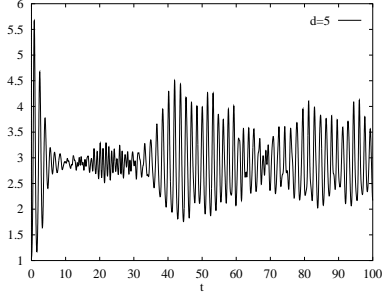


(d)  $d=20$

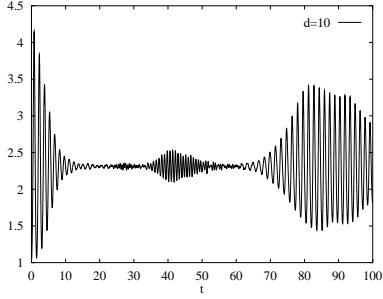
FIG. 7. Long-time behavior of the exact solution for Gaussian initial conditions with  $g_\infty = 1$ ,  $\bar{m}^2 = 2$ ,  $G_\infty = 1$ .



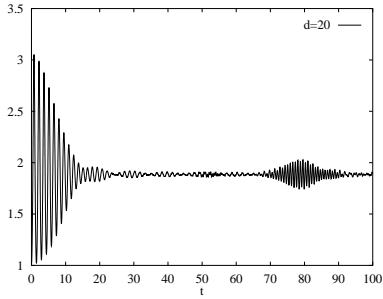
(a)  $d=1$



(b)  $d=5$



(c)  $d=5$



(d)  $d=10$

FIG. 8. Long-time behavior of the exact solution for Gaussian initial conditions with  $g_\infty = 20$ ,  $\bar{m}^2 = 21$ ,  $G_\infty = 1$ .

$d$	$g$	$G$	$m^2$	$\tilde{r}$	$r_0$
1	0.2320	1.3760	2.0000	0.9359	2.9359
5	0.5628	1.0572	1.9805	2.1877	4.1739
10	0.7266	1.0269	1.9315	3.1255	5.0638
20	0.8728	1.0129	1.8596	4.4451	6.2765
$\infty$	1.0000	1.0000	1.2500	$\sqrt{d-1}$	

TABLE I. Initial values for  $\bar{m}^2 = 2.0$ ,  $g_\infty = 1.0$

$d$	$g$	$G$	$m^2$	$\tilde{r}$	$r_0$
1	2.4363	1.3760	21.0000	0.9359	2.9359
5	5.9798	1.0572	20.9805	2.1877	4.1865
10	7.9590	1.0269	20.9315	3.1255	5.1199
20	10.0209	1.0129	20.8596	4.4450	6.4305
$\infty$	20.0000	1.0000	20.2500	$\sqrt{d-1}$	

TABLE II. Initial values for  $\bar{m}^2 = 21.0$ ,  $g_\infty = 20.0$